INDOOR AIR QUALITY

The human oxidation field

Nora Zannoni[1]*†, Pascale S. J. Lakey[2], Youngbo Won[3], Manabu Shiraiwa[2]*, Donghyun Rim[3]*, Charles J. Weschler[4,5], Nijing Wang[1], Lisa Ernle[1], Mengze Li[1]‡, Gabriel Bekö[4], Pawel Wargocki[4], Jonathan Williams[1,6]*

Hydroxyl (OH) radicals are highly reactive species that can oxidize most pollutant gases. In this study, high concentrations of OH radicals were found when people were exposed to ozone in a climate-controlled chamber. OH concentrations calculated by two methods using measurements of total OH reactivity, speciated alkenes, and oxidation products were consistent with those obtained from a chemically explicit model. Key to establishing this human-induced oxidation field is 6-methyl-5-hepten-2-one (6-MHO), which forms when ozone reacts with the skin-oil squalene and subsequently generates OH efficiently through gas-phase reaction with ozone. A dynamic model was used to show the spatial extent of the human-generated OH oxidation field and its dependency on ozone influx through ventilation. This finding has implications for the oxidation, lifetime, and perception of chemicals indoors and, ultimately, human health.

North Americans and Europeans spend, on average, ~90% of their time indoors (including home, workplace, and transport) (*1*, *2*). Within this enclosed space, occupants are exposed to a multitude of chemicals from various sources, including outdoor pollutants that penetrate indoors, gaseous emissions from building materials and furnishings, and products of human activities such as cooking and cleaning (*3*). In addition, the occupants themselves are a potent mobile source of gaseous emissions from breath and skin (human bioeffluents) as well as primary and secondary particles (*4*). Characterization of these indoor sources and the main indoor removal mechanisms are key to understanding indoor air quality (*5*).

Chemical removal of gas-phase species in outside air during daytime is mostly initiated by hydroxyl (OH) radicals, which are formed when a short-wavelength photolysis product of ozone (O_3) [an excited oxygen atom, O (^{1}D)] reacts with water. Longer-wavelength photolysis of nitrous acid (HONO) and formaldehyde (HCHO) also provides small additional OH sources outside, as does the light-independent ozonolysis of alkenes via Criegee intermediate formation (*6*). By contrast, the indoor environment is less influenced by direct sunlight, in particular ultraviolet light, which is largely filtered out by glass windows, so that primary production of OH indoors via O (^{1}D) is negligible. Although some OH can be generated by longer-wavelength artificial light by photolysis with natural light of formaldehyde and HONO if present, O_3 entering the building from outside is generally considered to be the principal oxidant indoors (*7*). Nevertheless, previous studies have highlighted the potential importance of alkene ozonolysis (*8*–*11*) in generating OH via Criegee intermediates in indoor environments, particularly when reactive molecules such as limonene from air fresheners or cooking are abundant. Previous estimates and measurements of indoor OH concentrations have ranged from 10^5 to 10^7 molecules cm^{-3}, which is substantially higher than outdoor nighttime concentrations and comparable to daytime atmospheric OH concentration levels in some regions (*8*–*15*).

None of the aforementioned model or measurement studies considered occupied indoor environments and therefore the underlying chemical influence of humans. Yet with every breath, humans exhale reactive alkenes such as isoprene, which can oxidize to further alkenes such as methyl vinyl ketone (MVK) and methacrolein (MACR) (*16*). Moreover, O_3 reacting at the skin surface with the skin-oil squalene ($C_{30}H_{50}$), a triterpene responsible for almost 50% of the unsaturated carbon atoms on human skin, releases a host of alkene-containing compounds to the air, including geranyl acetone, 6-methyl-5-hepten-2-one (6-MHO), OH-6-methyl-5-hepten-2-one (OH-6-MHO), 4-methyl-8-oxo-4-nonenal (4-MON), 4-methyl-4-octene-1,8-dial (4-MOD), and *trans*-2-nonenal (*17*). These species have the potential to react further in the gas phase, either to generate OH through reaction with O_3 or to deplete OH through direct reaction with the alkene. Therefore, humans have the potential to profoundly affect the oxidative environment indoors, particularly in areas of high occupancy (*18*), larger exposed body surface, and higher air temperature and humidity (*19*).

In this study, measurements were conducted in a climate-controlled stainless-steel chamber (see Fig. 1) with three different groups of four adult subjects on four separate days (including two replicates from the same group) (*20*). The air change rate (ACR) (3.2 hour^{-1}) and O_3 concentration [100 parts per billion (ppb) at the inlet and 35 ppb indoors] used in this experiment were chosen for reproducing a realistic scenario based on the expected O_3 decrease due to occupancy (*21*). (ACR is the number of times that the total air volume in a room or space is completely replaced by outdoor air in an hour.) From this data, we have determined the indoor concentrations and spatial distribution of OH radicals generated by humans upon exposure to O_3. This oxidative field is produced in isolation from other indoor sources or sinks of OH. A steady-state approach was applied, combining measured total OH reactivity (OH loss frequency in s^{-1}), measured concentrations of compounds containing an alkene double bond, and available literature values of OH yields from O_3 with alkene reactions. For comparison, the OH levels were also determined by an independent method using isoprene and its oxidation products. In the final step, the empirically derived OH levels and measurements were compared with those obtained from a detailed multiphase chemical kinetic model, and these results were used to simulate high spatial and time-resolved OH distributions in a room using a computational fluid dynamics (CFD) model. To investigate the existence and variability of spatial concentration gradients, we tested four scenarios: (i) an evaluation of the experimental results using the same underfloor air distribution from a perforated floor along with intensive air mixing at the average indoor O_3 concentration of 35 ppb as in the experiment, (ii) the same ventilation condition of the experiment without any mixing fans at an indoor O_3 concentration of 35 ppb to simulate a residential condition, (iii) air jets supplied at ceiling height and an indoor O_3 concentration of 35 ppb to simulate an office condition, and (iv) same as (iii) except the indoor O_3 concentration was 5 ppb.

Results

Total OH reactivity of human emissions

Figure 2 shows the OH loss frequency (total OH reactivity) measured directly in the chamber. The total OH reactivity of the gas-phase human bioeffluents was, on average, 8 ± 4 s^{-1} in the absence of O_3 and 34 ± 16 s^{-1} when O_3 was present (mean value ± measurement error, determined at equilibrium in the last 15 min before volunteers left the chamber). In the absence of O_3, the dominant OH sinks were reactive compounds in human breath (e.g., isoprene 64%), whereas in the presence of O_3,

[1]Atmospheric Chemistry Department, Max Planck Institute for Chemistry, Mainz, Germany. [2]Department of Chemistry, University of California, Irvine, CA, USA. [3]Department of Architectural Engineering, Pennsylvania State University, University Park, PA, USA. [4]International Centre for Indoor Environment and Energy, Environmental and Resource Engineering, DTU Sustain, Technical University of Denmark, Lyngby, Denmark. [5]Environmental and Occupational Health Sciences Institute, Rutgers University, Piscataway, NJ, USA. [6]Energy, Environment and Water Research Center, The Cyprus Institute, Nicosia, Cyprus.
*Corresponding author. Email: jonathan.williams@mpic.de (J.W.); nora.zannoni@mpic.de (N.Z.); m.shiraiwa@uci.edu (M.S.); dxr51@psu.edu (D.R.)
†Institute of Atmospheric Sciences and Climate, National Research Council, Bologna, Italy.
‡Department of Climate and Space Sciences and Engineering, University of Michigan, Ann Arbor, MI, USA.

the dominant OH sinks were reactive compounds generated by O_3 reactions with skin lipids such as 6-MHO (31%), 4-oxopentanal (4-OPA) (6%), and the sum of other aldehydes (29%) (*19*, *22*). Figure S1 shows the fractional contributions to OH reactivity for the various measured species. A comparison between the measured and calculated reactivities from the individually measured volatile organic compounds (VOCs) (Fig. 2) showed that the main reactive VOCs present in the chamber were quantified within the method uncertainties (total uncertainty for the measured OH reactivity is 48%; total uncertainty for the calculated OH reactivity is 30%) (*19*, *22*). This was a prerequisite for applying the steady-state method to determine OH using total OH reactivity and the combined OH sources.

OH radical concentration from the steady-state method

Table 1 reports the predominant alkenes of human origin measured in the presence of O_3, their OH production rates, and the resulting OH concentrations at steady state (see methods eq. S5). The empirically determined OH concentration from the four experiments involving three different groups of four adult human subjects was, on average, $(7.1 \pm 2) \times 10^5$ molecules cm^{-3}, whereas replicate experiments on the same group of subjects yielded $(7.16 \pm 0.07) \times 10^5$ molecules cm^{-3} (mean value ± 1σ). The values assume that the room is uniformly well mixed; therefore, the result represents the mean OH concentration within the chamber under the prevailing conditions: ventilation rate of 3.2 ± 0.11 $hour^{-1}$ and O_3 of 35 ppb with four people present. [Note that O_3 was equal to 100 ppb at the inlet and 95 ppb in the chamber before people entered (*20*).] For one of the four experimental days, Fig. 2 shows a time series of the calculated OH concentration from the onset of its generation (when O_3 is introduced into the chamber) to when the human bioeffluents reached steady-state conditions. Detailed information on the measured alkene concentrations, their reaction rate coefficients, and OH yields for the same experiment are provided in table S1, whereas fig. S2 shows the simplified reaction scheme of 6-MHO ozonolysis and respective product yields. The most important alkene for generating OH was found to be 6-MHO, followed by geranyl acetone, OH-6-MHO, limonene, 4-MON, and 4-MOD (fig. S3). By contrast, isoprene (OH yield 0.27) and the products resulting from isoprene reacting with OH (MVK plus MACR) made a negligible contribution. Most of the alkenes responsible for generating OH result from the ozonolysis of skin lipids. Notably, the same molecule, 6-MHO, is both the strongest chemical source of OH radicals (fig. S3) and the predominant sink for OH under these conditions (fig. S1).

OH radical concentration from the precursor-product method

Figure 2 also shows the concentration of OH determined by an alternative approach (see methods eq. S6), namely, using a precursor (isoprene) and product [mass-to-charge ratio (*m*/*z*) 71.049, here reported as *m*/*z* 71, which represents the sum of the products generated from the reaction between isoprene and OH and which is considered here as solely MVK plus MACR; see methods and supplementary text and (*23*)]. In the presence of O_3, a ~4-fold increase of the *m*/*z* 71 mixing ratio was observed (fig. S4), which is primarily due to isoprene oxidation by OH (isoprene fractional loss of 0.16%) with a small contribution from gas-phase ozonolysis (isoprene fractional loss of 0.012%). The mean OH concentration obtained is 1.2×10^6 molecules cm^{-3}, which is close to, but higher than, the value obtained from eq. S5 (Fig. 2). The agreement between the measured and calculated OH reactivities reported in Fig. 2 precludes the possibility that an unmeasured alkene is the cause. A second possibility is that the OH yields and rate coefficients used in eq. S6 overestimate the OH radicals generated from human emissions. A sensitivity test (table S2) was therefore conducted on the result from eq. S6, where each input variable was varied within its confidence interval. This indicated that the variables that most influence the OH concentration are the isoprene oxidation product yields (relative change 19 to 31%) and the ratio between isoprene oxidation products and isoprene concentrations (relative change 19%). Therefore, any fragment interfering in the measurement of *m*/*z* 71 would result in a higher OH concentration as determined through eq. S6. However, in a separate experiment, it was noted that some *m*/*z* 71 signal was generated from the O_3 exposure of four clean shirts (without people). Detailed results on the OH reactivity of people wearing short and long clothing and of solely clothing were discussed in Zannoni *et al.* (*19*). We therefore deduce that the precursor-product method overestimated the OH radical abundance because of interfering emissions of the product from the clothing. Nevertheless, it should be noted that there is broad agreement between the two OH estimates and that the values derived for human-generated OH are substantial and highly meaningful in the indoor environment.

Table 1. OH production rates of the measured alkenes and OH concentrations. OH radical production rates of isoprene, 6-MHO, OH-6-MHO, limonene, MVK plus MACR, 4-MON, 4-MOD, geranyl acetone, and *trans*-2-nonenal (in units of molecules cm^{-3} s^{-1}) and OH concentrations (in units of molecules cm^{-3}) obtained with the steady-state method from measurements of alkenes and OH reactivity of four adult volunteers. The data reported in each column were obtained from experiments on separate days, under the same conditions, and within the same campaign. A1, A2, and A3 indicate different groups of subjects. A2(1) and A2(2) were replicates of the same experiment with the same group of volunteers. LOD, limit of detection.

Compound *i*	A1	A2(1)	A2(2)	A3
Isoprene	3.61×10^5	3.06×10^5	3.07×10^5	4.10×10^5
6-MHO	1.22×10^7	1.57×10^7	1.66×10^7	1.82×10^7
OH-6-MHO	1.67×10^6	1.72×10^6	2.35×10^6	2.72×10^6
Limonene	7.52×10^5	below LOD	8.78×10^5	7.28×10^5
MVK plus MACR	7.59×10^3	5.46×10^3	8.34×10^3	1.17×10^4
4-MON	below LOD	5.25×10^4	5.61×10^5	2.87×10^5
4-MOD	below LOD	below LOD	6.05×10^5	3.40×10^5
Geranyl acetone	1.96×10^6	2.13×10^6	2.44×10^6	2.07×10^6
trans-2-nonenal	1.17×10^5	9.39×10^4	1.76×10^5	1.42×10^5
OH	$(4.2 \pm 1) \times 10^5$	$(7.2 \pm 2) \times 10^5$	$(7.1 \pm 2) \times 10^5$	$(9.7 \pm 3) \times 10^5$

Modeled OH radical field in the occupied environment

The measured alkene concentrations, OH concentration, and OH reactivity were simulated with the detailed kinetic model KM-SUB-Skin-Clothing (*24*, *25*) (figs. S5 and S6). Outputs from the kinetic model were then used in a CFD model to simulate the human OH radical field (*26*, *27*). The OH radical field in the chamber due to the presence of the people within was determined for four different conditions. The results of OH reactivity and OH concentration under steady-state conditions with O_3 present (before the occupants left the chamber, at 360 min elapsed time from the beginning of the experiment) are reported in Fig. 3 for all four simulations.

The first condition (Fig. 3A) allows direct comparison with the measured results: air and O_3 are supplied from a simulated perforated floor, and two virtual fans mix the air inside the chamber (as represented in Fig. 1). The maximum air velocity occurs at the chamber

walls, and the maximum air temperature occurs at the human-body surface, whereas around the subjects, the air velocity and temperature are uniformly distributed (fig. S7). With O_3 present, the largest source of OH reactivity is the human-body surface (Fig. 3Ai), with O_3-squalene–generated carbonyls such as 6-MHO being the predominant contributors to the OH reactivity. The maximum modeled OH reactivity is 50 s^{-1}, whereas the mean chamber value is ~35 s^{-1}, in good agreement with the measured value. The spatial distribution of the OH radicals generated by the occupants has the opposite distribution to the OH reactivity; their concentration is highest in the room air and lowest at the body surface (Fig. 3Aii). The mean OH concentration under steady-state conditions is 1×10^6 molecules cm^{-3}, which agrees well with the values inferred from the two independent empirical methods described in the prior sections "OH radical concentration from the steady-state method" and "OH radical concentration from the precursor-product method."

The second condition investigates the impact of the reduced air mixing by suppressing the virtual fans and simulating a more realistic scenario of a typical residence without active mixing (Fig. 3B). A buoyancy-driven flow pattern then developed because of the low-momentum air supply from the floor level and convective flow generated by the heat of the seated occupants. In this case, air movement is mainly driven by temperature gradients associated with indoor heat sources, as seen in fig. S9, which shows the corresponding air temperature and velocity distributions. Without active air mixing, both air temperature and velocity have a clear vertical gradient, with the room air temperature being highest near the chamber ceiling and with the maximum air speed around the body surface of the occupants (fig. S9). Therefore, a strong vertical gradient of OH reactivity is generated from the floor (low) to ceiling (high), as shown in Fig. 3B. Air temperature, velocity, and airflow pattern determine the evolution of the OH reactivity field shape, forming a reactive cloud around and above the mouth of the occupants that prolongates above the head of the occupants (Fig. 3Bi) in the convectively rising air plume. Accordingly, the vertical profile of OH radical concentration is opposite to that of OH reactivity, showing a maximum at the chamber floor (Fig. 3Bii). The maximum modeled OH reactivity and OH concentration values were 50 s^{-1} and 2×10^6 molecules cm^{-3}, respectively. Under such conditions, the lifetime of the OH radical is 20 ms above a person's head, increasing to 100 ms toward the floor.

The third condition investigates how the vertical gradient is affected by the location of the incoming air and O_3 source. Air and O_3 are supplied from a jet diffuser at ceiling height,

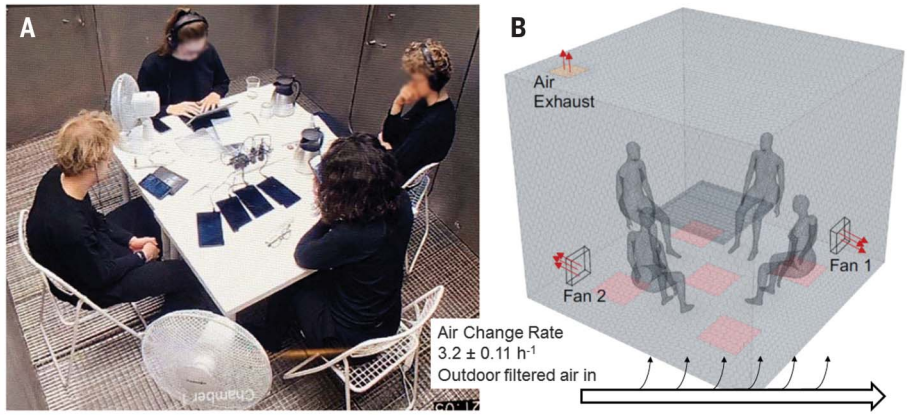

Fig. 1. Photo of one experiment and CFD model framework. (**A**) Photograph of the occupied stainless-steel climate chamber at the Technical University of Denmark (DTU). (**B**) Framework of the experiment used for the CFD modeling. Ambient air is introduced through the entire floor and exhausted via one air outlet in the ceiling.

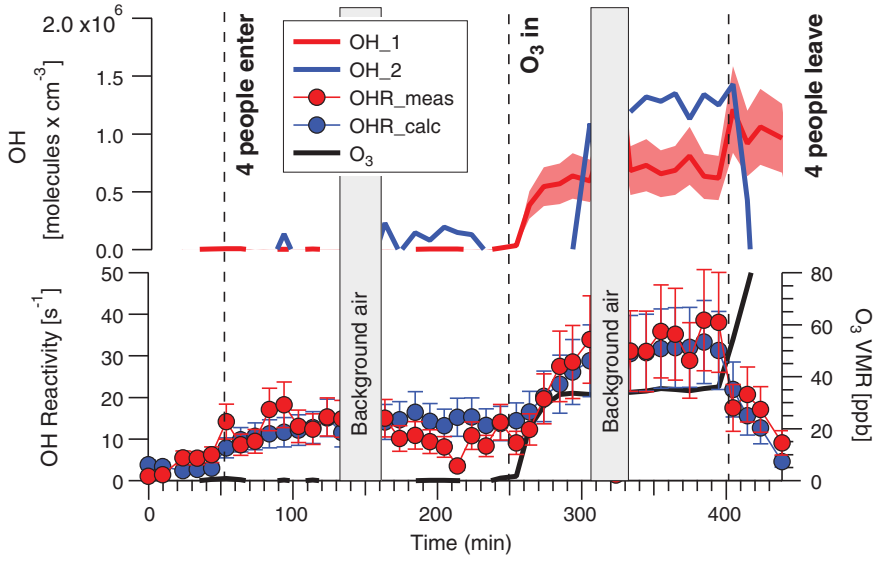

Fig. 2. Time series of OH concentration, OH reactivity, and O_3 concentrations. Time series of OH concentration (top) and measured OH reactivity (OHR_meas), calculated OH reactivity (OHR_calc), and O_3 (bottom) for one selected experiment. OH concentration was determined by two independent methods: (i) OH_1 (steady-state method), from the OH production rate through ozonolysis of alkenes and the measured total OH reactivity and (ii) OH_2 (precursor-product), using the lifetime of isoprene. VMR, volume mixing ratio.

as in a realistic scenario of a typical office. In this case, the maximum OH reactivity is again reached at the body surface and above people's heads, with minimum levels close to the air-O_3 inlet (Fig. 3Ci). The maximum OH concentration is now displaced to the air-O_3 inlet, although still caused by the interaction of O_3 with 6-MHO (Fig. 3Cii).

The fourth case investigates the spatial gradient using the conditions applied in the third case but with lower indoor O_3 concentration (5 ppb). This is the median reported O_3 indoor concentration from a number of residences, schools, and offices during occupancy (*28*). As shown in Fig. 3D, the OH reactivity (Fig. 3Di) and OH concentrations (Fig. 3Dii) are reduced to ~20 s^{-1} and ~3×10^4 molecules cm^{-3}, respectively, whereas the spatial gradients are qualitatively very similar to those of the original simulations with higher O_3. In all the investigated conditions, humans exposed to O_3 generated an indoor OH oxidation field around them.

Discussion

This study has experimentally and theoretically determined with consistent results that substantial OH concentrations are generated in indoor environments owing to the presence of humans and O_3. Using an OH production rate based on measured alkenes and simultaneous direct measurements of OH reactivity, the

steady-state approach yielded OH concentrations under equilibrium conditions of $(7.1 \pm 2) \times 10^5$ molecules cm^{-3}, whereas the precursor-product yielded 1.2×10^6 molecules cm^{-3}. Under the conditions of the bare chamber experiments (ACR of 3.2 ± 0.11 $hour^{-1}$ and O_3 of ~35 ppb), the oxidation field generated by one adult is ~1.8×10^5 molecules cm^{-3}.

These results show that humans exposed to O_3 generate a substantial OH oxidizing field around them. The OH radical levels are sufficiently high to outcompete the more abundant but slower O_3 reactions that are now assumed to dominate organic compound oxidation in the indoor environment. Isoprene, for example, under this chamber's experimental conditions, is predominantly oxidized by OH.

Notably, the OH concentrations derived in this study are of the same order of magnitude as the OH concentrations measured or modeled in previous indoor studies (*8*–*15*) that were conducted without people present (Table 2). This suggests that the OH oxidizing field strength generated by human occupants is comparable to that resulting from all other indoor sources of alkenes. In this context, it is important to note that humans are mobile and so represent a displaceable chemical source and oxidation field indoors. Furthermore, it is shown that within indoor environments, strong spatial gradients in OH concentration can develop, with the direction depending on the location of the O_3 source and ventilation. Such pronounced spatial gradients have been reported in indoor experiments previously, with OH levels varying with degree of illumination (*12*), with trace gases showing strong gradients around the breathing zone (*29*), and, during cooking, with markedly different VOC levels occurring between floor and ceiling (*30*). Under real-world conditions, the occupied space can be influenced by additional heat sources such as those from incoming light or hot cooking surfaces that will further affect the spatial gradients observed. Spatial and temporal scales of indoor constituents are modulated by rates of chemical reactions, surface interactions, and building ventilation; short-lived compounds, including OH radicals, can exhibit sharp spatial gradients because their temporal scales are determined mainly by reaction rates and are only marginally affected by deposition and ventilation rates (*31*).

Key to the generation of OH around humans is the presence of reactive alkenes generated from the reaction of O_3 with various components of skin oil (e.g., squalene), particularly 6-MHO but also geranyl acetone, OH-6-MHO, 4-MON, and 4-MOD. Because of its extremely rapid reaction with OH [rate coefficient of the reaction 6-MHO with OH ($k_{6\text{-MHO+OH}}$) = 1.57×10^{-10} cm^3 $molecules^{-1}$ s^{-1}, which is faster than that of isoprene] and its high measured yield of OH upon ozonolysis [0.75 (*32*)], 6-MHO was found to be the most important OH source and OH sink. As such, it should be included in future modeling and measurement studies of indoor environments. Previous studies have measured or estimated the indoor OH concentration based on OH generated from the ozonolysis of alkenes from nonhuman sources (*8*–*10*) and OH produced from HONO photolysis (*12*, *14*). Weschler and Shields focused on the importance of terpenes from scented products to generate OH in an indoor environment (*8*, *9*), and Carslaw calculated that typically ~90% of OH indoors is produced from alkene ozonolysis, whereas only ~10% is generated from HONO photolysis (*13*). Gómez Alvarez *et al.* showed that when sunlight shines directly into an unoccupied classroom, HONO photolysis is the main source of OH indoors, measuring peaks of OH up to 1.8×10^6 molecules cm^{-3} during the highest photolysis period (*12*). The relative importance of these human- and nonhuman-related OH sources will depend critically on the conditions of the specific indoor environment, including lighting, outdoor and indoor sources, temperature, humidity, and, as demonstrated here, people. The human-induced OH field will also interact with other indoor sources and surfaces, including emissions from floors, walls, furnishings, and scented products (which were excluded on purpose in our study). In real-world environments, O_3 can also react with squalene in settled dust, on skin flakes, and on skin oil–soiled surfaces such as clothes, generating 6-MHO and further influencing the OH oxidation field, even

Table 2. Comparison between this study and previous direct and indirect measurements and estimates of OH concentration in indoor environments. FAGE, fluorescence assay by gas expansion; MCM, master chemical mechanism.

OH concentration (molecules cm^{-3})	O_3 concentration (ppb)*	Method	Notes	Reference
$(7.1 \pm 2) \times 10^5$	35, 100	Measured OH reactivity	Four adult occupants	This study
4×10^6 to 2×10^7	20, 40	OH direct measurements with FAGE	No occupants	Carslaw *et al.* (*43*)
3×10^5 to 3.5×10^6	5, 180	OH direct measurements with FAGE	No occupants, cleaning products and maximum O_3 present	Bloquet *et al.* (*14*)
1.8×10^6	5, 30	OH direct measurements with FAGE	No occupants, daytime maximum level	Gómez Alvarez *et al.* (*12*)
6.5×10^4 to 3.7×10^5	1.6, 4.8	Tracer decay measurement	No occupants	White *et al.* (*15*)
4.6×10^5	60, 120	Constant emission of a tracer measurement	No occupants, detergents present	Singer *et al.* (*10*)
4×10^5	12, 37	Estimate from detailed chemical model based on the MCM	No occupants	Carslaw (*13*)
1.2×10^5	20, 200	Estimate based on SAPRC-99 chemistry model	No occupants	Sarwar *et al.* (*11*)
$(7.1 \pm 0.8) \times 10^5$	62, 192	Constant emission of a tracer measurement	No occupants	Weschler and Shields (*9*)
1.7×10^5	20†	Estimate based on steady-state mass-balance model	No occupants	Weschler and Shields (*8*)

*Values represent O_3 indoor concentration followed by O_3 outdoor concentration †O_3 indoor concentration

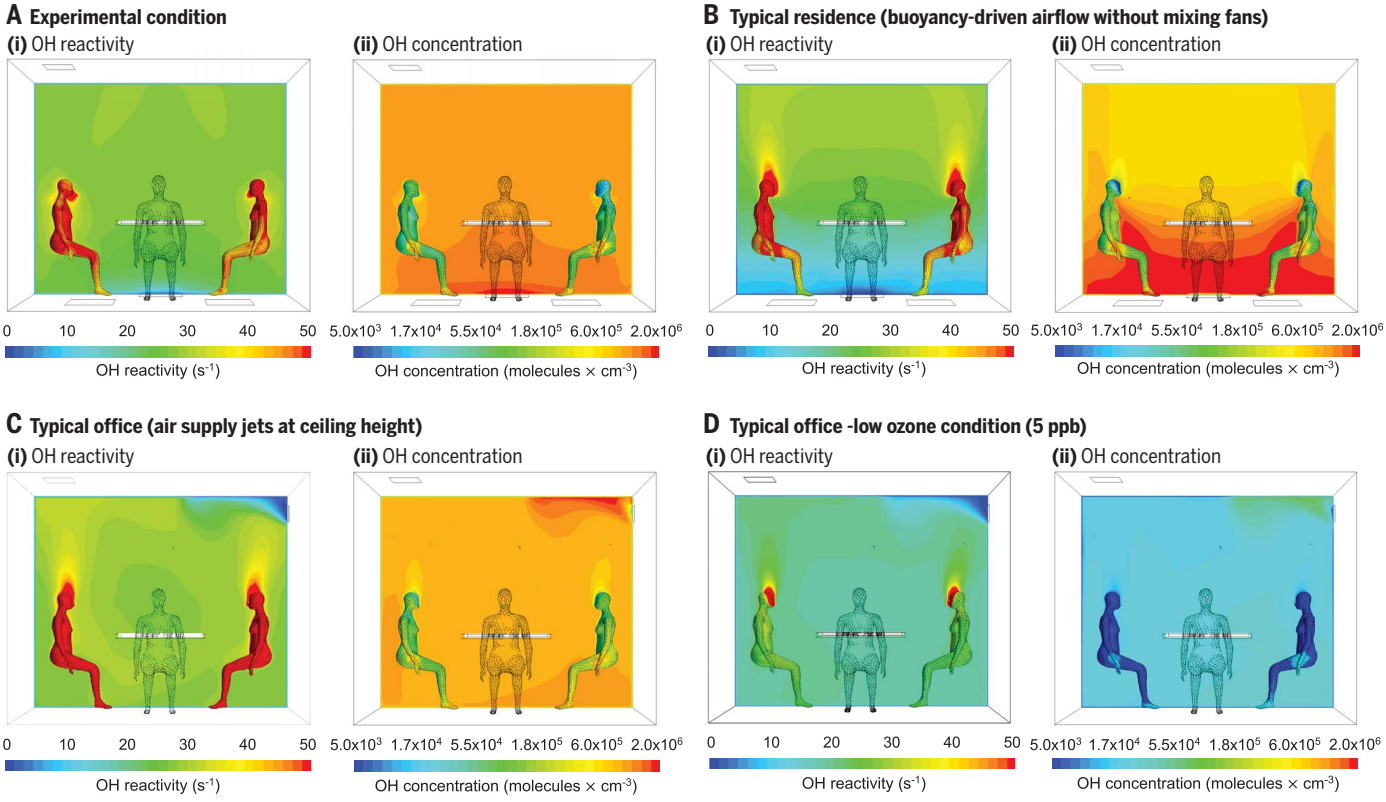

Fig. 3. Spatial distribution of OH reactivity and OH concentration at elapsed time 360 min (before people left the chamber). (**A**) Simulation of the experiment with two indoor mixing fans and inflow through the floor to match the experimental conditions. (**B**) Simulation with no virtual mixing by fans for typical conditions. (**C**) Simulation of inflow from an upper supply inlet of a wall. (**D**) Simulation with lower (5 ppb) O_3 from an upper supply inlet.

without people being present. Liu *et al.* (*18*) showed that such reactions are still detectable after 5 days without occupancy by measuring squalene oxidation products. Zhang *et al.* (*33*) estimated the "off-body" skin-oil contribution from the aforementioned experiment. Collectively, squalene and three squalene-derived oxidation products (which can be a source of secondary 6-MHO) contributed 2.7 μmol of double bonds per square meter of surface in this residence.

Previous studies have shown that exposure to natural light indoors has a large effect on OH generation (*12*). Carslaw simulated an OH concentration of 9×10^4 molecules cm^{-3} for indoor winter conditions in a home environment with artificial light (*13*), which is similar to the value obtained from our study when O_3 was absent. However, such levels are small in comparison to the human-induced concentrations found in our study when O_3 was present. The indoor O_3 concentration is therefore a critical parameter in determining the strength of the human-generated oxidation field (*8*–*10*). This in turn is dependent on the outdoor O_3 concentration and ventilation rates of the indoor space. Real-world indoor environments, including offices and homes, typically have lower ventilation rates (*21*) than that of our study. Moreover, the availability of multiple surfaces for O_3 reactions provided by furnishings will further lower indoor O_3 concentrations below those used here (*7*). At an ACR of 3 $hour^{-1}$, one would expect indoor O_3 concentrations that are roughly 50% of outdoor values. At an ACR of 1 $hour^{-1}$, one would expect indoor O_3 concentrations that are roughly 25% of outdoor values (*21*). Hence, although an indoor O_3 level of 40 ppb is high, it does occur when outdoor levels are high and the ACR is moderate to high. Median O_3 levels for residences, offices, and classrooms are ~5 ppb (*28*), and this scenario is represented by the simulation of Fig. 3D, i and ii. Therefore, the OH concentrations associated with the human oxidation field reported from our experimental case (Fig. 3A, i and ii) likely represent upper limits. However, even with lower O_3 concentrations, substantial OH fields will establish wherever humans are exposed to O_3, which is virtually all indoor and outdoor environments. In addition to generating OH radicals, the reaction of O_3 with skin-surface lipids also produces nanocluster aerosols (*34*).

The human OH radical oxidation field may play an important role in the detection of chemical cues because oxidation gradients near the body surface can attenuate and transform odor signals, affecting odor perception. Indeed, it was recently shown that molecules that react rapidly with the OH radical are generally more sensitively detected by the human nose (*35*). Growing research is reporting the role of chemical signals in human communication (*36*).

In indoor environments, O_3 reacts primarily with organic compounds that contain carbon-carbon double bonds. This is typically about 10% of the total number of organics detected in indoor air. The OH radical is a less-discriminating oxidant and reacts rapidly with almost all organics present in indoor air. A number of the measured products cannot be explained by O_3 chemistry; they can only be explained by OH radical chemistry. In essence, this study reveals a cascade of oxidation pathways that lead to many more oxidation products (present at higher concentrations) than would be present if O_3 were the sole oxidant.

The chemistry revealed in this study has health implications. These include the acute and chronic health impacts of certain OH-oxidation products whose toxicities have been evaluated [e.g., methacrolein (*37*)]. However, there exists a large set of reaction products with unevaluated toxicities. Knowledge about this

underlying chemistry and its products can guide us toward selecting compounds for which toxicity data should be generated. This group may include compounds that adversely affect human health. The fact that products are generated in the vicinity of the breathing zone (see Fig. 3) amplifies these concerns. Over the past decade, there have been considerable advances in our knowledge of the products derived from indoor O_3 chemistry (*38*).

Products of such chemistry include short-lived species such as stabilized Criegee intermediates, OH radicals, hydroperoxyl radicals, and alkylperoxy radicals, as well as more stable products such as hydrogen peroxide, organic hydroperoxides, peroxy acids, organic nitrates, and secondary organic aerosols (*39*–*41*) (see extended discussion in the supplementary materials). The interactions among the human oxidation field, the convective heat transfer (thermal plume), the chemical mass transfer around a human body, and the generation of a personal reactive cloud (*42*) warrant further research regarding the human health implications. The different conditions simulated in this study can be particularly useful to evaluate potential mitigation strategies. This study shows that in the presence of O_3, humans both emit and oxidize chemical compounds in their immediate environment, a process that affects all indoor environments.

REFERENCES AND NOTES

1. N. E. Klepeis *et al*., *J. Expo. Anal. Environ. Epidemiol.* **11**, 231–252 (2001).
2. European Commission, Press corner; https://ec.europa.eu/commission/presscorner/home/en.
3. D. K. Farmer *et al*., *Environ. Sci. Process. Impacts* **21**, 1280–1300 (2019).
4. C. J. Weschler, *Indoor Air* **26**, 6–24 (2016).
5. W. W. Nazaroff, A. H. Goldstein, *Indoor Air* **25**, 357–361 (2015).
6. B. J. Finlayson-Pitts, J. N. Pitts, *Chemistry of the Upper and Lower Atmosphere* (Elsevier, 2000).
7. A. P. Ault *et al*., *Chem* **6**, 3203–3218 (2020).
8. C. J. Weschler, H. C. Shields, *Environ. Sci. Technol.* **30**, 3250–3258 (1996).
9. C. J. Weschler, H. C. Shields, *Environ. Sci. Technol.* **31**, 3719–3722 (1997).
10. B. C. Singer *et al*., *Atmos. Environ.* **40**, 6696–6710 (2006).
11. G. Sarwar, R. Corsi, Y. Kimura, D. Allen, C. J. Weschler, *Atmos. Environ.* **36**, 3973–3988 (2002).
12. E. Gómez Alvarez *et al*., *Proc. Natl. Acad. Sci. U.S.A.* **110**, 13294–13299 (2013).
13. N. Carslaw, *Atmos. Environ.* **41**, 1164–1179 (2007).
14. M. Blocquet *et al*., in vol. 1 of *14th International Conference on Indoor Air Quality and Climate (INDOOR AIR 2016)* (International Society of Indoor Air Quality and Climate, 2016), pp. 1310–1317.
15. I. R. White *et al*., *Environ. Sci. Technol.* **44**, 6269–6274 (2010).
16. A. Amann *et al*., *J. Breath Res.* **8**, 034001 (2014).
17. A. Wisthaler, C. J. Weschler, *Proc. Natl. Acad. Sci. U.S.A.* **107**, 6568–6575 (2010).
18. Y. Liu *et al*., *Proc. Natl. Acad. Sci. U.S.A.* **118**, e2018140118 (2021).
19. N. Zannoni *et al*., *Environ. Sci. Technol.* **55**, 13614–13624 (2021).
20. G. Bekö *et al*., *Indoor Air* **30**, 1213–1228 (2020).
21. W. W. Nazaroff, *Indoor Air* **31**, 282–313 (2021).
22. N. Wang *et al*., *Environ. Sci. Technol.* **55**, 149–159 (2021).
23. J. C. Rivera-Rios *et al*., *Geophys. Res. Lett.* **41**, 2014GL061919 (2014).
24. P. S. J. Lakey *et al*., *Indoor Air* **27**, 816–828 (2017).
25. P. S. J. Lakey *et al*., *Commun. Chem.* **2**, 56 (2019).
26. D. Rim, E. T. Gall, S. Ananth, Y. Won, *Build. Environ.* **130**, 40–48 (2018).
27. Y. Won, P. S. J. Lakey, G. Morrison, M. Shiraiwa, D. Rim, *Indoor Air* **30**, 1229–1240 (2020).
28. W. W. Nazaroff, C. J. Weschler, *Indoor Air* **32**, e12942 (2022).
29. P. V. Nielsen, C. Xu, *Indoor Built Environ.* **31**, 1420326X2110485 (2021).
30. G. Shen *et al*., *Environ. Pollut.* **267**, 115493 (2020).
31. P. S. J. Lakey *et al*., *Commun. Chem.* **4**, 110 (2021).
32. A. M. Smith, E. Rigler, E. S. C. Kwok, R. Atkinson, *Environ. Sci. Technol.* **30**, 1781–1785 (1996).
33. M. Zhang, Y. Gao, J. Xiong, *Chemosphere* **291**, 132772 (2022).
34. S. Yang *et al*., *Environ. Sci. Technol.* **55**, 14536–14545 (2021).
35. J. Williams, A. Ringsdorf, *Philos. Trans. R. Soc. London Ser. B* **375**, 20190274 (2020).
36. S. C. Roberts, J. Havlíček, B. Schaal, *Philos. Trans. R. Soc. London Ser. B* **375**, 20190258 (2020).
37. New Jersey Department of Health, Workplace health and safety: Hazardous substances; https://www.nj.gov/health/workplacehealthandsafety/right-to-know/hazardous-substances/.
38. Committee on Emerging Science on Indoor Chemistry, Board on Chemical Sciences and Technology, Division on Earth and Life Studies, National Academies of Sciences, Engineering, and Medicine, *Why Indoor Chemistry Matters* (National Academies Press, 2022).
39. C. J. Weschler, *Environ. Health Perspect.* **114**, 1489–1496 (2006).
40. C. J. Weschler, N. Carslaw, *Environ. Sci. Technol.* **52**, 2419–2428 (2018).
41. J. P. D. Abbatt, C. Wang, *Environ. Sci. Process. Impacts* **22**, 25–48 (2020).
42. R. L. Corsi, J. Siegel, A. Karamalegos, H. Simon, G. C. Morrison, *Atmos. Environ.* **41**, 3161–3165 (2007).
43. N. Carslaw, L. Fletcher, D. Heard, T. Ingham, H. Walker, *Indoor Air* **27**, 1091–1100 (2017).

ACKNOWLEDGMENTS

We thank S. Langer for measuring NO. N. Ziersen, T. Klüpfel, and R. Hofmann are acknowledged for their support. We thank the volunteers for participating in the study. **Funding:** This work was funded by Alfred P. Sloan Foundation grants G-2018-11233 (J.W., G.B., and P.W.), G-2019-12306 (M.S. and D.R.), and G-2020-13912 (M.S. and D.R.). **Author contributions:** Conceptualization: J.W., G.B., P.W., C.J.W., N.Z.; Methodology: J.W., N.Z., C.J.W., M.S., P.S.J.L., D.R., Y.W., G.B., P.W.; Investigation: N.Z., J.W., P.S.J.L., M.S., Y.W., D.R., C.J.W., N.W., L.E., M.L., G.B., P.W.; Visualization: N.Z., J.W., P.S.J.L., M.S., Y.W., D.R.; Funding acquisition: J.W., G.B., P.W., M.S., D.R.; Project administration: J.W., G.B., P.W., M.S., D.R.; Supervision: N.Z., J.W., M.S., D.R.; Writing – original draft: N.Z., J.W.; Writing – review and editing: All authors. **Competing interests:** The authors declare that they have no competing interests. **Data and materials availability:** All data are available in the main text or the supplementary materials.

SUPPLEMENTARY MATERIALS

science.org/doi/10.1126/science.abn0340
Materials and Methods
Supplementary Text
Figs. S1 to S9
Tables S1 to S5
References (*44*–*62*)
Data S1

Submitted 7 November 2021; accepted 7 July 2022
10.1126/science.abn0340